AIAA JOURNAL
Vol. 36, No. 4, April 1998

Flow Characterization in the ONERA F4 High-Enthalpy Wind Tunnel

Philippe Sagnier* and Jean-Luc Vérant†
ONERA, 92320 Châtillon, France

Experimental results obtained in the ONERA F4 hot-shot wind tunnel have been analyzed to address two important problems for this type of wind tunnel, i.e., the determination of reservoir conditions and the thermochemical nature of the nozzle flow. Numerical tools (one-dimensional and two-dimensional inviscid or viscous, unsteady or space marching codes) are used to reproduce the results of the high-enthalpy experiments. To illustrate this approach, several runs are investigated with different arc-chamber material options, for which diode laser infrared absorption spectrometry (DLAS) has provided freestream velocity, translational temperature, and nitric oxide concentration measurements. The reservoir enthalpy can be determined using spherical and sharp-cone probe heat-transfer-rate measurements with adequate correlations. Recent direct measurements of freestream velocity with electron beam fluorescence time-of-flight technique are used to cross check DLAS and heat-transfer-rate probe results. Concerning the thermochemical nature of F4 nozzle flows, an unexpected conclusion is obtained, as the nozzle wall pressure and translational temperature are observed to be close to equilibrium values at high-enthalpy operating conditions. A thermochemical model is proposed, involving vibration–dissociation–recombination coupling, which seems able to reproduce available experimental data.

Nomenclature

A	= area of a nozzle cross section
A^*	= nozzle throat area
H_i	= reservoir enthalpy
H_w	= enthalpy at wall conditions
K_e	= chemical-reaction equilibrium constant
k_b	= backward chemical-reaction rate
k_f	= forward chemical-reaction rate
M_∞	= freestream Mach number
P	= static pressure
P_i	= reservoir pressure
P_i'	= pitot pressure
Q	= heat flux
Q_{stag}	= stagnation-point heat flux
R	= perfect-gas constant (288.2 J/kg/K for air)
R_{nose}	= nose radius
Re_∞	= freestream unit Reynolds number per meter
RP	= rarefaction parameter for a length of 1 m, $M_\infty / Re_\infty^{0.5}$
s	= curvilinear abscissa
T	= translational temperature
T_a	= averaged temperature
T_v	= vibrational temperature
T_0	= reference temperature, 273.15 K
t	= time
U	= velocity
x	= abscissa
γ	= isentropic expansion exponent

Introduction

THE ONERA F4 wind tunnel (Fig. 1) was built in the early 1990s to simulate the atmospheric re-entry of hypersonic vehicles. It is a hot-shot type, meaning that the settling conditions are obtained by heating the test gas with an electric arc in an arc chamber. The energy is delivered by an impulse generator, at a power of up to 150 MW for several tens of milliseconds. The settling-chamber pressure P_i can be as high as 500 bar, and the reduced total enthalpy H_i / RT_0 can be as high as 250 (about 20 MJ/kg). After the arc-chamber conditions reach the desired levels, the arc is stopped and the nozzle throat is opened by igniting a pyrotechnic plug to initiate the nozzle flow. The blowdown is interrupted by firing a pyrotechnic valve in the arc chamber, quickly evacuating the remaining gas into a dump tank. Run duration of up to 400 ms can be achieved but with reservoir conditions decreasing with time. However, reservoir pressure and enthalpy decays are slow enough (1%/ms) to allow force measurements to be performed. The useful run period is established after a perturbed period of 30 ms because of the throat-plug-expelling phase.[1] Synthetic air and pure nitrogen are used as test gases. F4 can be equipped with four different contoured nozzles with an area ratio varying from 1850 to 32,000. Nozzle 2, with an area ratio of 4490, a length of 3.4 m, and an exit diameter of 0.7 m, was used for most of the aerothermal tests reported here.

In this type of wind tunnel, the reservoir pressure can be measured directly in the arc chamber but not the reservoir enthalpy. In effect, unlike the shock tunnels for which the enthalpy can be determined from shock velocity measurement, the total enthalpy in hot-shot tunnels can be deduced only from indirect measurements of heat-transfer rates or freestream velocity.

The work performed in the F4 facility to determine the reservoir enthalpy and the knowledge gained during this investigation about the thermochemical nature of the nozzle flow are described. As shown, the present work demonstrates the need for numerical simulations with sophisticated physical models, even for flows around simple geometries, to correctly describe the features of the high-enthalpy flow phenomena. Because of the large number of parameters contained in such gas flows, only a numerical and parametrical strategy allows the extreme limits of thermochemical and fluid mechanical assumptions to be simulated before deeper investigations.

The first part of the paper describes the work on reservoir enthalpy determination for two different arc chambers, one made of copper and the other made of carbon. The thermochemistry of the nozzle flow is then discussed.

Reservoir Enthalpy Determination

The experimental campaign based on the Hyperboloïd-flare (H-flare) model tests[1,2] led to a disagreement between computed and measured heat-flux values. Initially it was believed that the total enthalpy in the F4 facility could be determined from equilibrium computations of the arc-chamber gas, using the known pressure and density. But the H-flare campaign analysis has demonstrated that this approach is not viable because of the thermal nonuniformity of the arc-chamber gas at high enthalpy. The thermal nonuniformity was

Presented as Paper 96-2239 at the AIAA 19th Advanced Measurement and Ground Testing Technology Conference, New Orleans, LA, June 17–20, 1996; received March 8, 1997; revision received Nov. 13, 1997; accepted for publication Nov. 23, 1997.

*Research Engineer, Fundamental and Applied Energetics Department, 29, Avenue de la Division Leclerc. E-mail: sagnier@onera.fr.

†Research Engineer, Fundamental and Applied Energetics Department, 29, Avenue de la Division Leclerc. E-mail: verant@onera.fr.

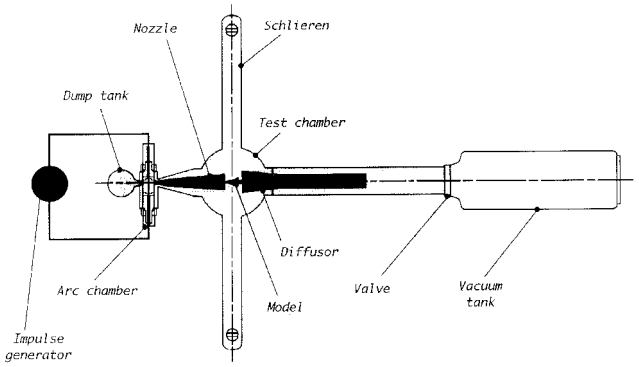

Fig. 1 F4 hot-shot wind tunnel.

identified from the discrepancy between the theoretical and experimental heat-flux values: The numerical heat fluxes were far lower than measurements. The calculated reservoir enthalpy was two or three times smaller than the enthalpy inferred from pitot pressure and the heat transfer rates to a model placed in the test section. After expending a considerable effort along this line, the method was abandoned in favor of the heat-transfer method described later.

The total enthalpy for F4 can be deduced from four types of measurements: stagnation-point heat-transfer rate for a spherical probe, heat-transfer rate for a slender sharp cone, velocity measurement by Doppler effect on NO spectra obtained with the diode laser infrared absorption spectrometry (DLAS) technique, and direct electron beam fluorescence (EBF) velocity time-of-flight measurement with the pseudospark electron gun.

Stagnation Heat-Flux Spherical Probes

To determine the reservoir enthalpy, first the heat-transfer rates are measured in the stagnation region of spherical catalytic probes. Correlating about 60 Navier–Stokes computations for stagnation-point heat fluxes, assuming nonequilibrium (catalytic wall) and perfect-gas flows, led to the following enthalpy–heat flux relationship[3]:

$$\frac{Q_{\text{stag}}\sqrt{R_{\text{nose}}/P_i'}}{[(H_i - H_w)/RT_0]^{1.069}} = 23.79 = \text{const} \pm 12\% \qquad (1)$$

where all variables are in SI units. The exponent and constant in Eq. (1) were obtained with a least-squares fitting of the numerical heat fluxes. It was demonstrated that, for perfect gas, the Fay–Riddell formula[4] can be simplified to the same form.[3] Correlations similar to Eq. (1) also were proposed for flight results.[3,5] Note that Eq. (1) implies no knowledge of the freestream properties, which are a source of uncertainty at high enthalpy. Furthermore, this correlation also can be employed to normalize heat-transfer distributions over models[1] at least as well as the scheme proposed by Miller.[6] Using Eq. (1), the F4 total enthalpy is monitored in situ by two heat-transfer spherical probes of 30- and 15-mm diam located at the nozzle exit. The uncertainty on spherical probe enthalpy determination is about ±20% when summing experimental and correlation uncertainties.

The spherical probes' surface-temperature/heat-flux data reduction takes into account the two-dimensional conduction effect, assuming a surface heat-flux distribution from Lees,[7] and temperature effect on wall thermal properties.[8] Efforts were made to characterize the effect of surface catalycity, as was done previously by Pope[9] for nitrogen flows. However, several metallic surface coatings produced no significant differences,[10] which is probably due to contamination plating of probe stagnation regions (these tests were performed with the first arc chamber, made of copper-based materials). Analyses showed that this stagnation-region plating was composed mostly of metals, e.g., copper, tungsten, and zirconium present as components of arc-chamber parts.[11] A heat-flux measurement technique, weakly sensitive to this contamination problem, then was studied.

Sharp-Cone Heat-Transfer Probe

The presence of either gaseous or solid impurities during shots could shift measured sphere stagnation heat transfer to higher values than could be expected. These effects are not well known but seem to be more complicated than simple solid particles impacting the model surface. It was observed that the walls of blunt models,[12] set at low angles of attack, were free of dust blasting or deposits. Therefore, a cone with 5-deg half-angle was chosen to augment the total enthalpy measurement (Fig. 2). Four surface coaxial thermocouples are set at three axial locations on the cone wall, made of the same material as the spherical probes, i.e., constantan.

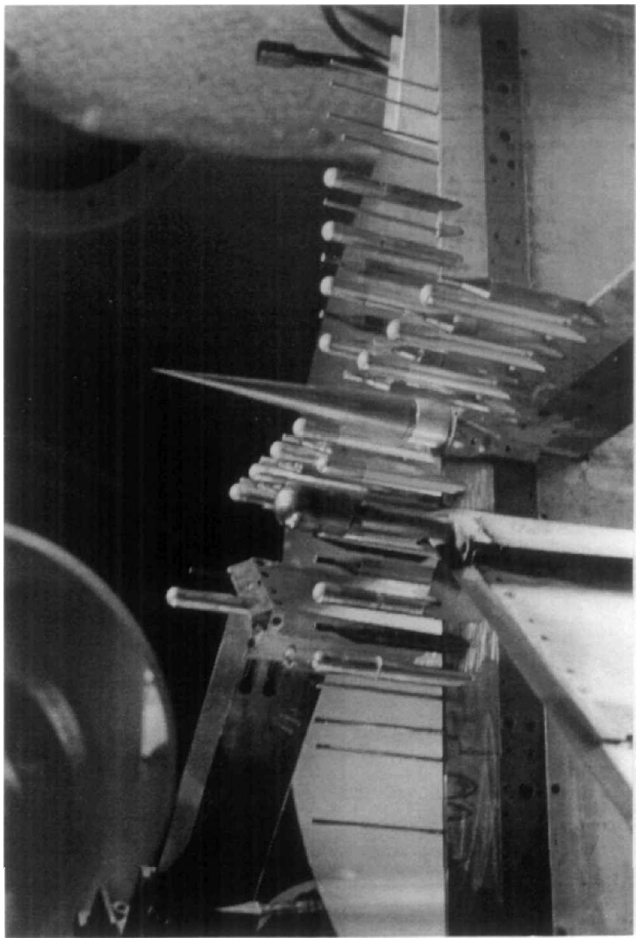

Fig. 2 Five-degree-half-angle sharp-cone probe on the cross rake in F4 test section, with pitot tubes and heat-flux spherical probes.

A few experiments have been performed with the sharp-cone model. Two runs labeled 760 and 762 (high-pressure, high-enthalpy condition) were made with different chambers (copper or carbon). The conventional chamber with copper–tungsten electrodes, copper liner and baffle, and organic insulators was used in the first test (760), and the carbon chamber with graphite electrodes, carbon–carbon liner, baffle, and insulators was used for the second test (762). Because carbon materials are able to withstand higher thermal stresses than the materials used previously, it was expected that flow contamination would decrease and hence probe measurements would be more accurate. Indeed, nozzle contamination has been reduced as shown by smoother measurement traces and fewer deposits on the impacting targets (mass reduction of up to one order of magnitude).

Experimental results for the runs with the cone—760 and 762—are displayed in Figs. 3 and 4. These figures show the evolution of the total enthalpies given by the spherical probes and the cone as a function of time for high-pressure and high-enthalpy conditions for two runs. The procedure employed in this case is based mainly on the use of computations: For convenience, we have established a correlation for each of the three thermocouple locations from a set of 10 parabolized Navier–Stokes laminar heat-transfer predictions,[13] assuming thermochemical nonequilibrium and fully catalytic wall. These correlations involved heat flux, pitot pressure, and total enthalpy normalization as

$$\frac{Q}{[(H_i - H_w)/RT_0]^{\beta}(P_i')^{\mu}} = \lambda \pm 2\% \qquad (2)$$

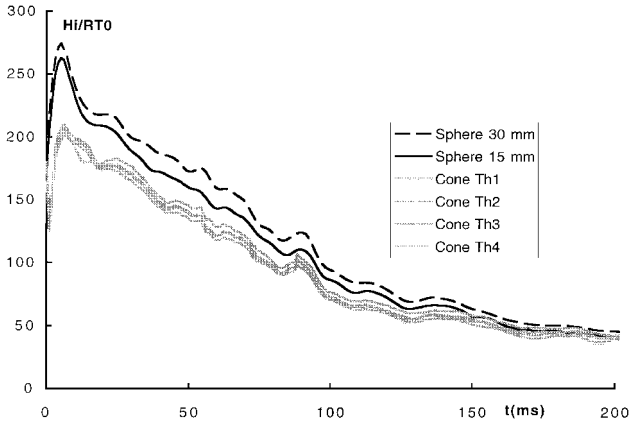

Fig. 3 Reduced reservoir enthalpy vs time for run 760 with copper chamber. The enthalpy is determined by both spherical probes (15- and 30-mm diam) according to Eq. (1) and a conical probe with four thermocouples according to Eq. (2).

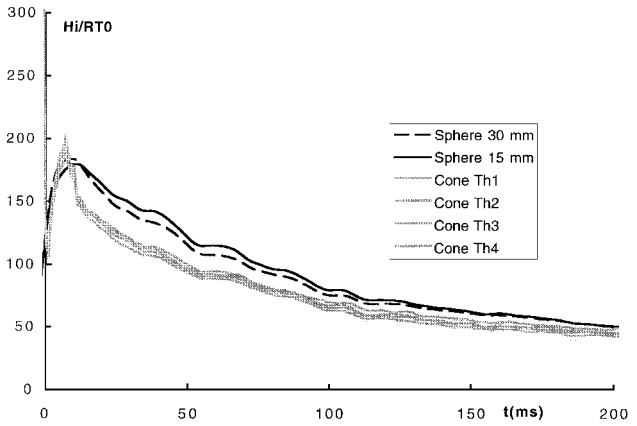

Fig. 4 Reduced reservoir enthalpy vs time for run 762 with carbon chamber.

where notations are the same as in Eq. (1). Coefficients β, μ, and λ depend on thermocouple axial location. Equation (2) correlates the numerical heat fluxes within $\pm 2\%$.

Probe Results

Figures 3 and 4 show the difference between enthalpies given by the sharp cone and the spherical probes for the copper and carbon chambers. The difference is largest at the beginning of the run when the flow contamination is likely to be at its maximum. Indeed, it is known[1,14] that most of the contamination occurs in the first 30 ms. In the case of the carbon chamber, this behavior is less obvious (Fig. 4). The difference between the two spherical probes (Figs. 3 and 4) also is thought to originate from the contamination because the carbon-chamber configuration seems to reduce this difference (Fig. 4). The four cone curves from the four cone thermocouples exhibit scattering of up to 15% at the beginning of the run, but there is less scattering with the carbon chamber. Finally, the temporal variation is much smoother with the carbon chamber than with the copper chamber, leading to the least scattering among the different heat-transfer probes (particularly spherical probes). Reduced sensitivity of the cone measurements to flow contamination is demonstrated during the first 30–40 ms of the runs, regardless of the chamber option chosen. However, the matching of enthalpies from the sharp cone and the spherical probes might have occurred earlier than indicated in Figs. 3 and 4, at least in the case of the carbon chamber (low contamination). The reason for these differences is not known, and this will require further investigation. At least this is not caused by test-section enthalpy radial gradient, as shown next. (Spherical probes are on the core side, and the cone is on the axis.)

Recently, the carbon arc chamber was improved (better carbon–carbon material and better design of some parts than for run 762).[15,16] The good agreement on the reservoir enthalpies obtained from measurements over probes with diameters of 15, 30, and 70 mm

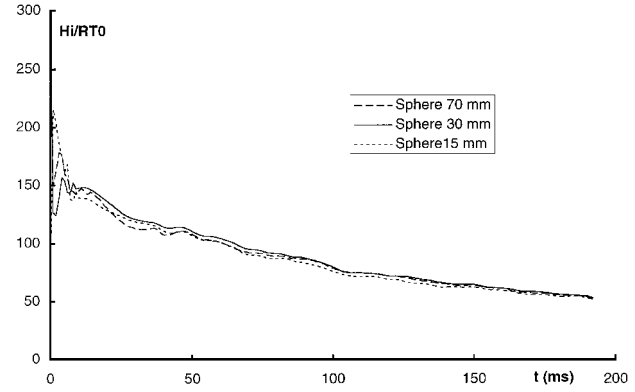

Fig. 5 Reduced reservoir enthalpy vs time for run 834 with carbon chamber for 15-, 30-, and 70-mm-diam probes.

(no sharp cone was used here) confirms the improvement reached on the flow contamination by using carbon materials (Fig. 5). The 70-mm probe is in fact the nose of a sphere-cone model (the Electre sphere-cone described later) located on the nozzle axis, showing that no significant enthalpy radial gradient affects the test section.

Another positive direct yield is that carbon parts such as the liner can be used for about 10 times more runs than copper parts. Use of the carbon arc chamber also presents some drawbacks. With the same impulse-generator-setting parameters, the reservoir enthalpy obtained with the carbon chamber is lower than with the copper chamber; this is probably due to the superior heat storage capability of carbon. Carbon parts normally can withstand 4000 K before ablation, compared to 1000 K for copper. The F4 domain remains to be reexplored with the carbon arc chamber.

DLAS and EBF Measurements

A previous calibration campaign with the DLAS technique was performed in 1994. The DLAS technique can provide the freestream velocity within $\pm 5\%$, the translational temperature within $\pm 30\%$, and the NO concentration within $\pm 30\%$ (Ref. 17). These data are obtained through the analysis of the absorption spectra of an infrared laser beam crossing the test section. Both velocity and translational temperature can be used to determine the reservoir enthalpy by making some assumptions about the flow thermochemical state.[8] Other DLAS results were compared with different nozzle flow models.[14,17–19] The enthalpy values were significantly lower than those obtained by spherical probes for the case of the copper chamber at the beginning of the runs, at least partly because of the influence of flow contamination on heat-flux measurements. With the carbon arc chamber, this disagreement on velocity is seen to be smaller, though it is still present at the beginning of the run. Note also that, in the past,[20,21] optical techniques already gave velocity values lower than those deduced from heat-transfer probes. Recently, with the carbon arc chamber further improved,[15,16] DLAS and spherical-probe freestream velocity results were successfully compared with the EBF time-of-flight technique.[18,19] The results are discussed in the following section.

Thermochemical Nature of Nozzle Flow

To determine the freestream flow properties, several types of measurements can be compared with theoretical calculations, i.e., nozzle and model wall-pressure distributions, pitot pressure profiles, freestream velocity, translational temperature, and NO concentration. For this purpose, nozzle exit-flow charts have been constructed[22] in which the thermochemical conditions at the nozzle exit are given in the a priori extreme limits of thermochemical and fluid mechanical assumptions. This task has been performed for two reasons: first, to explain the unsuccessful attempt[23] to match the experimental pitot pressure and nozzle wall pressure with the values calculated from the nonequilibrium and turbulent-boundary-layer assumptions; and second, to know freestream similitude parameters for model testing. These six nozzle flowcharts were computed by taking into account the following airflow models: six combinations of equilibrium, nonequilibrium, frozen core flow with laminar turbulent nozzle boundary layer for reduced enthalpies varying from

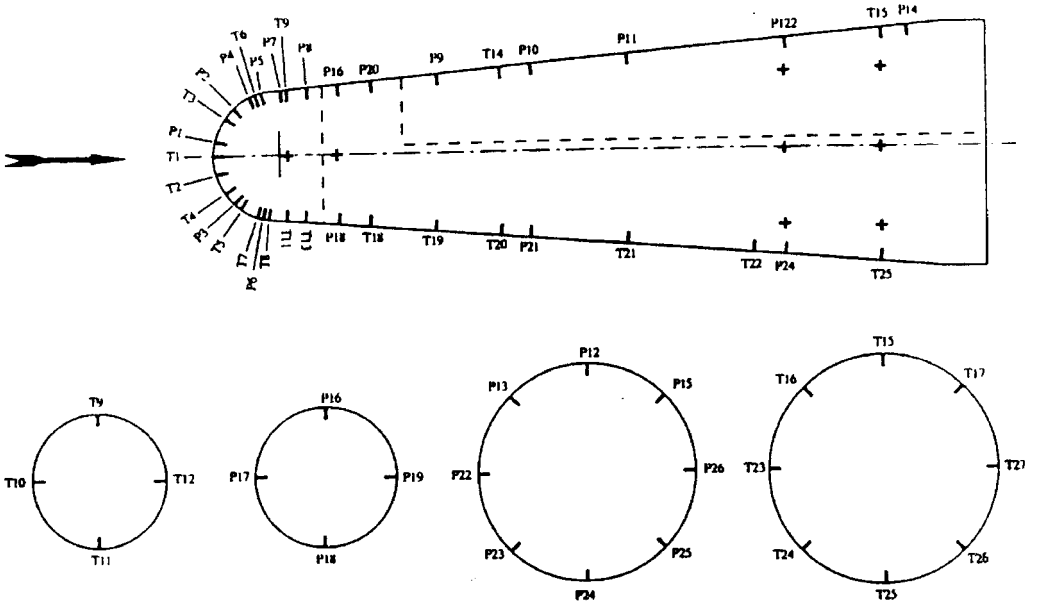

Fig. 6 Schematic of Electre model and instrumentation.

30 to 330 and pressures varying from 50 to 1000 bar. For each of the six charts, 77 nozzle computations have been performed.

Two-dimensional viscous computations also were performed, to rebuild either nozzle flows or flows around models such as the Electre sphere-cone (Fig. 6). In particular, it was shown that the pressure distribution along the low-angle (cone half-angle of 4.5 deg) conical part of such models is sensitive to the freestream Mach number.[12,19,24,25] Electre wall-pressure measurements then can yield valuable information on the freestream properties.

One-Dimensional Computational Tools

The basic tool to build the nozzle-flowcharts was the one-dimensional Euler package TUYEQ-TURGE[26] with an iterative coupling consisting of a turbulent-boundary-layer model of Edenfield[27] or an integral laminar boundary layer. TUYEQ is a one-dimensional equilibrium Euler code that uses a tabulated Mollier diagram, taking into account virial effects at high pressures. It is used to compute the flow in the convergent part of the nozzle for all cases and the entire nozzle flow for equilibrium cases. TURGE, the one-dimensional thermochemical nonequilibrium Euler code, is started a few centimeters downstream of the nozzle throat for nonequilibrium and frozen calculation cases. The modeling of thermochemistry is of great importance for nozzle exit data, such as static pressure, translational temperature, and Mach number, as shown later in this section.

Two-Dimensional Computational Tools

To refine the one-dimensional results, nozzle flow computations can be performed with two-dimensional techniques. The axisymmetric computations for the F4 nozzle were performed with the ONERA three-dimensional parabolized Navier–Stokes (PNS) code PANASCE.[28,29] The implemented physical models allow perfect-gas, equilibrium, and nonequilibrium thermochemical viscous flow simulations. Turbulent nozzle flow predictions are made using the Baldwin–Lomax algebraic model. Calculation was repeated with several explicit schemes from the literature, such as those of Van Leer,[30] Yee and Harten,[31] Osher and Solomon,[32] and hybrid upwind splitting[33] (HUS) method. The last two schemes are used most often for nozzle computations because of their superior ability in boundary-layer calculation with no numerical dissipation. Second-order accuracy is achieved with the MUSCL technique. An implicit algorithm is applied to the PNS steady solver using an iterative technique with substeps in each step-marching section to achieve the required accuracy based on pressure and temperature. To take advantage of the speed of the PNS computation, an approximate solution is constructed at the starting location in the vicinity of the throat where the flow begins to be supersonic. This technique, which is applied at the throat in place of the usual unsteady solver solution, is based on a small perturbation theory of inviscid transonic flow, written

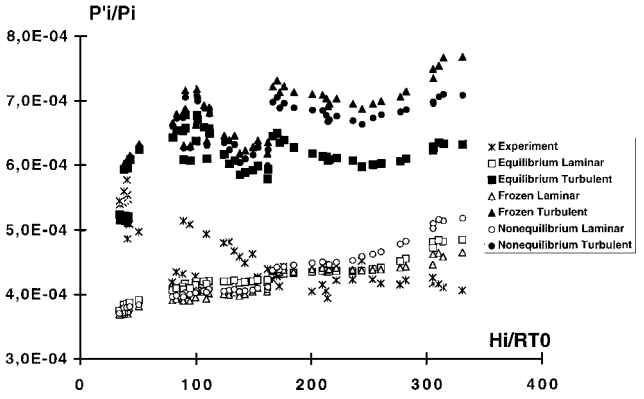

Fig. 7 H-flare campaign: pitot/reservoir pressure ratio vs reduced reservoir enthalpy for different thermochemical and boundary-layer models.

by Carrière[34] for $\gamma = 1.4$, which was recently extended to arbitrary γ. The assumption of a constant γ is approximately correct for the present flow.[35] The nozzle computational technique, using the PNS solution initialized with the small perturbation theory, was tested extensively against full unsteady solutions in a prior endeavor.[35] The favorable results gave confidence for the nozzle flow calculation.

Flows around axisymmetric models placed in the test section have been computed[1,2,24] with ONERA two-dimensional unsteady Navier–Stokes codes, either in perfect gas (HOMAR[36]) or in thermochemical nonequilibrium (CELHYO[37]). To save computational time, PNS solutions also can be used downstream of the model nose subsonic region.

Pressure

The wall and pitot pressures, normalized by the reservoir pressure,[1,2] have been compared with the different nozzle flowcharts in Figs. 7 and 8, respectively. The wall pressure is measured, in particular, at the exit of nozzle 2 at two points and then averaged. In Figs. 7 and 8, the theoretical data are obtained by interpolating with the reservoir pressure and enthalpy into the charts. The experimentally obtained pitot pressure values (accuracy of $\pm 5\%$) agree best with the turbulent-flow assumption at low enthalpy and with the laminar-flow assumption at high enthalpy. Furthermore, the measured wall pressures at the nozzle exit flowfield seem to agree with an equilibrium assumption at high enthalpies. (Pressure measurement accuracy at nozzle exit is about $\pm 10\%$.) This pressure behavior observed through a one-dimensional analysis prompted us to investigate further using the more sophisticated two-dimensional method described in the preceding section.

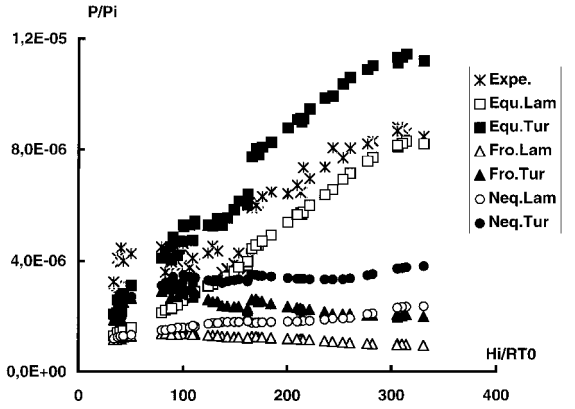

Fig. 8 H-flare campaign: nozzle-wall/reservoir pressure ratio vs reduced reservoir enthalpy for different thermochemical and boundary-layer models.

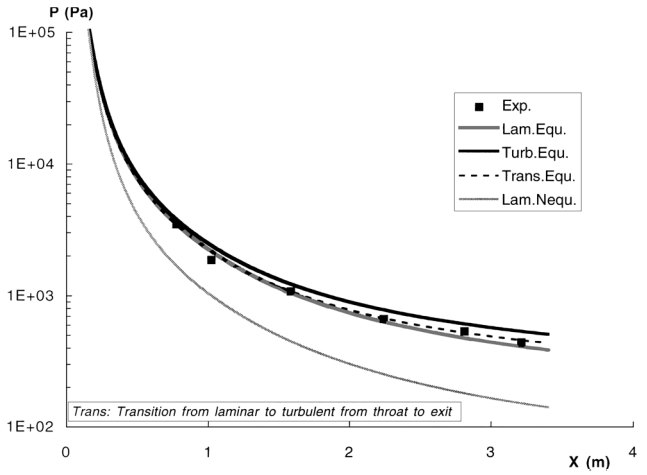

Fig. 9 Nozzle-2 wall-pressure distributions (copper chamber, $P_i = 430$ bar, $H_i/RT_0 = 260$): experiment vs PNS computations assuming laminar, transitional, turbulent-equilibrium, or laminar-nonequilibrium flows.

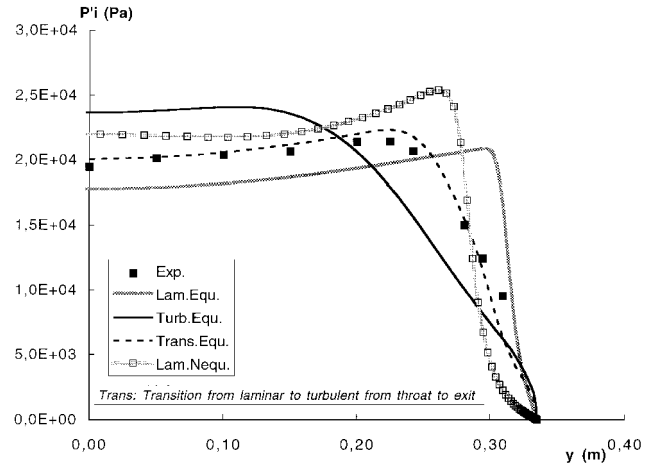

Fig. 10 Pitot-pressure profile at 14 cm downstream of nozzle-2 exit (copper chamber, $P_i = 430$ bar, $H_i/RT_0 = 260$): experiment vs PNS computations assuming laminar, transitional, turbulent-equilibrium, or laminar-nonequilibrium flows.

To confirm the analysis yielded by one-dimensional results, two-dimensional computations, using the PNS solution initialized with the small-perturbation theory, were performed, in particular for the following cases: a copper chamber at $P_i = 430$ bar, $H_i/RT_0 = 260$ (Refs. 14 and 38), and a carbon chamber (in its most recent version) at $P_i = 404$ bar, $H_i/RT_0 = 170$ (Refs. 18 and 19). The results are displayed in Figs. 9–13. For thermochemical nonequilibrium, the chemical kinetics (5 species, 17 reactions) is from Park,[39] and

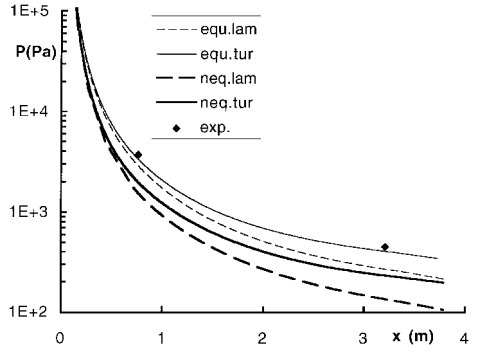

Fig. 11 Nozzle-2 wall-pressure distributions (carbon chamber, $P_i = 404$ bar and $H_i/RT_0 = 170$): experiment vs PNS computations assuming laminar and turbulent, equilibrium and nonequilibrium flows.

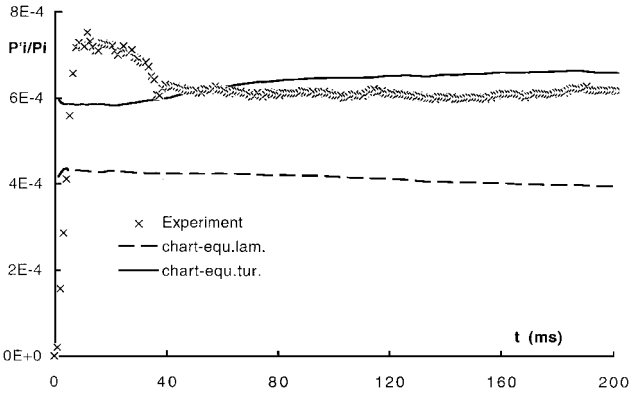

Fig. 12 Nozzle-2 pitot/reservoir pressure ratio time trace for a carbon chamber run: experiment vs one-dimensional computations assuming laminar and turbulent, equilibrium flows.

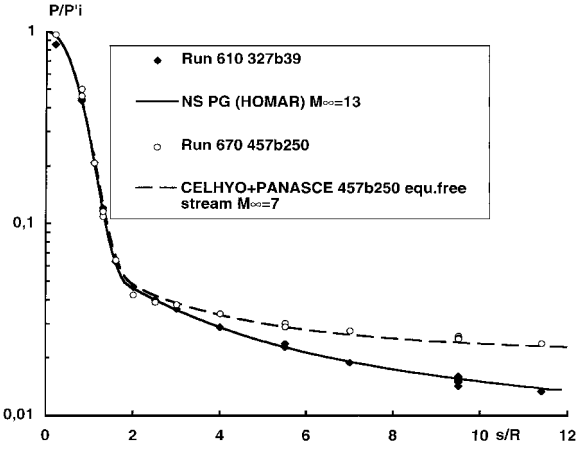

Fig. 13 Low- and high-enthalpy copper chamber runs: Electre wall-pressure/nose-pressure ratio distribution compared with viscous computations at $M_\infty = 13$ and 7.2 (low-enthalpy case, $P_i = 327$ bar, $H_i/RT_0 = 39$; high-enthalpy case, $P_i = 457$ bar, $H_i/RT_0 = 250$).

the vibrational kinetics on nitrogen and oxygen is from Millikan and White.[40] Nozzle wall pressure and pitot pressure comparisons in Figs. 9 and 10 show that the two-dimensional results lead to the conclusion that, at high enthalpy, the core flow seems to be close to equilibrium and the nozzle boundary layer is in a transitional regime. These results are the same as those obtained from the one-dimensional calculations. The transitional behavior assumed in the calculation of the boundary-layer flow (transition from the throat to the exit) may not necessarily be the true behavior of the flow. However, the pitot pressure profile in Fig. 10 is consistent with the assumed behavior, as it could be for unit Reynolds number far below 10^6 (D. Arnal, ONERA, Toulouse, France, private communication, 1996). For the case in Figs. 9 and 10, the unit Reynolds number at the nozzle exit equals 5.5×10^4 and 1.65×10^5 for equilibrium and nonequilibrium, respectively. The corresponding

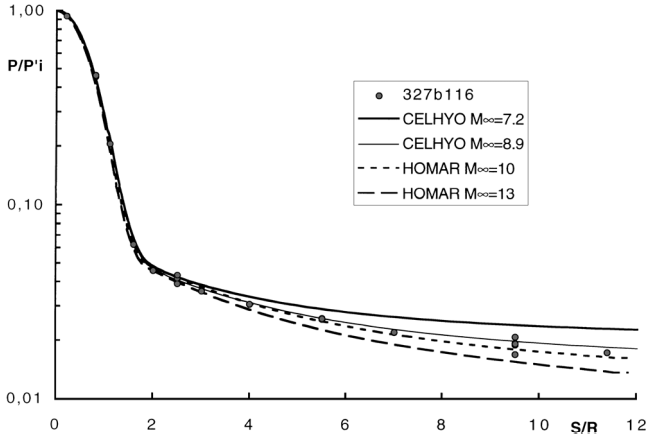

Fig. 14 High-enthalpy carbon-chamber run ($P_i = 327$ bar, $H_i/RT_0 = 116$): Electre wall-pressure/nose-pressure ratio distribution compared with viscous computations at $M_\infty = 13$, 10, 8.9, and 7.2.

rarefaction parameter *RP* values are 0.031 and 0.032. Most of the runs under high-pressure, high-enthalpy conditions appear to be in the transitional regime, with a few exceptions of purely laminar and purely turbulent flows.

The next example (Fig. 11) confirms that the nozzle wall-pressure distribution seems to be close to equilibrium. (Only two pressure taps were plugged in.) At the time of 40 ms, the nozzle boundary layer is closest to the turbulent calculation, as indicated also by pitot-pressure time traces compared with nozzle-flow data in Fig. 12. (No calibration rake was used because the H-flare model was present.) The unit Reynolds number at nozzle exit equals 1.4×10^5 and 2.8×10^5 for equilibrium and nonequilibrium, respectively, and corresponding *RP* values are 0.023 and 0.024.

At that point of the discussion, such a proximity to equilibrium of the nozzle wall pressure was observed with a full repeatability and regardless of the arc chamber option, copper or carbon. Figure 8 indicates that nozzle-wall-pressure experimental/theoretical comparison does not yield any problem at low-enthalpy conditions (see also Ref. 23), where all thermochemical models give about the same results. We do not see any reason to mistrust the nozzle-wall-pressure measurements in the high-enthalpy regime. In particular, if some systematic errors artificially increase the values of the measured pressures, it also would be the case under low-enthalpy conditions where, in particular, the same *RP* as at high enthalpy can be reproduced. Furthermore, a validation of these nozzle-wall-pressure measurements is given by the analysis of the wall-pressure distribution over the Electre sphere-cone model.[12,18,19] As stated earlier, the pressure distribution over the Electre sphere-cone is sensitive to the freestream Mach number. Figures 13 and 14 display the comparisons of Electre wall-pressure distributions with Navier–Stokes computations at different freestream Mach numbers for copper-chamber and carbon-chamber runs, respectively. In the range of reservoir conditions presented in Figs. 13 and 14, the largest uncertainty on the pressure measurements is for the aftbody taps, of the order of ±10% (Ref. 12). Figure 13 shows that, for the copper chamber, the Electre low-enthalpy pressure distribution agrees with the computation at $M_\infty = 13$, the M_∞ value given by any nozzle flowchart. At high enthalpy (Fig. 13), the best agreement is obtained with the computation at $M_\infty = 7.2$, the M_∞ value given by the equilibrium assumption (about 13 for nonequilibrium). If some uncertainty can affect the reservoir enthalpy determination for copper runs, carbon runs confirm the copper results. An example is given in Fig. 14, where the Electre experimental pressure distribution agrees best with the $M_\infty = 8.9$–10 computations, values again given by the equilibrium assumption. A test-section freestream Mach number close to equilibrium will yield a translational temperature and a static pressure also close to equilibrium (mass-flow conservation and equation of state). Electre wall-pressure results are in agreement with the nozzle-wall-pressure results. Optical measurement results have to be analyzed before making conclusions on the nozzle-flow thermochemical nature.

Optical measurements were performed with the DLAS technique (freestream velocity by Doppler effect, translational temperature, NO concentration) and with the EBF velocimetry technique (freestream velocity by time-of-flight measurement at ±5%). For simplicity, only one run, with the latest carbon arc chamber, is considered. The repeatability of the measurements is very good, regardless of the arc-chamber option (copper or carbon), with respect to the uncertainty on the enthalpy determination in the case of the copper arc chamber.[8,12,18,19]

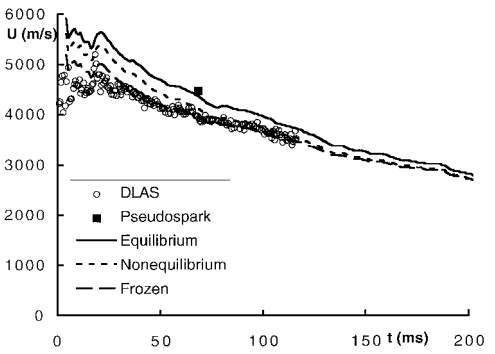

Fig. 15 Carbon-chamber run 842: velocities vs time from DLAS, pseudospark, and different flow models (from the charts entered with reservoir pressure, 30-mm probe enthalpy, and pitot pressure).

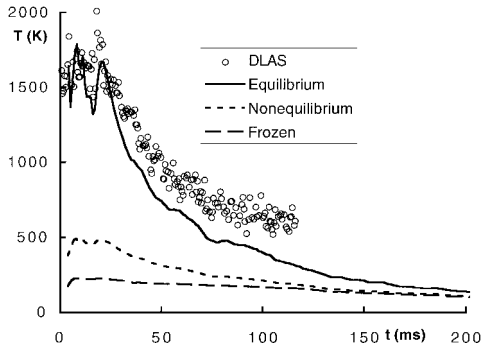

Fig. 16 Carbon-chamber run 842: translational temperature vs time from DLAS and different flow models.

Freestream Velocity

Freestream velocities obtained by different means are compared along an H-flare carbon-chamber run[18,19] in Fig. 15. Experimental results come from the DLAS technique and the EBF velocimetry technique. For the latter, only one measurement is obtained during the run, the pulsing capability of the pseudospark gun remaining to be tested. These results are compared with three models from the nozzle flowcharts, equilibrium, nonequilibrium, and frozen-flow assumptions. The interpolating data were the reservoir pressure, the 30-mm probe enthalpy (same as the one computed from the model heat-flux distribution and very close to the 15-mm probe, i.e., within 10%), and the pitot pressure (to get rid of the boundary-layer displacement-thickness influence on the nozzle-flow expansion rate[18]). The uncertainty on the yielded velocities is about ±10% (half the enthalpy uncertainty). Taking into account the uncertainties, all results are in good agreement and it is difficult to determine which is the best thermochemical model. The velocity is a parameter weakly sensitive to the thermochemistry. Generally, DLAS data seem to be closest to the frozen or nonequilibrium assumptions, and the pseudospark velocity is about the same as, or slightly larger than, the DLAS velocity. Nevertheless, such good velocity comparisons add to the problem of the reservoir enthalpy determination, which can be considered now as solved: When using the carbon arc chamber, all of the determination techniques of reservoir enthalpy–freestream velocity are in agreement.

Freestream Translational Temperature

The freestream translational temperature is much more sensitive to flow thermochemistry than the velocity, as shown by Fig. 16. Here, the thermochemical assumption that is closest to DLAS data is undoubtedly the equilibrium flow, also if taking into account the uncertainties (same as for the enthalpy for thermochemical models,

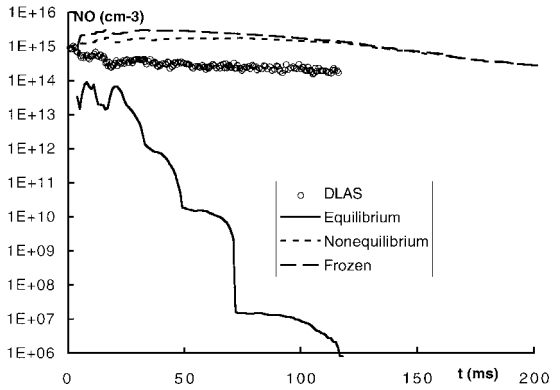

Fig. 17 Carbon-chamber run 842: NO concentration vs time from DLAS and different flow models.

i.e., ±20%). The DLAS technique gives even translational temperatures that are larger than equilibrium temperatures. This is a general trend for the carbon-chamber runs. (For copper, it is the same trend when considering the overestimation of spherical-probe enthalpy due to flow contamination.)

Freestream NO Concentration

Time evolutions of NO concentration (in molecules/cm^3) are displayed in Fig. 17. DLAS results are much closer to frozen and nonequilibrium assumptions than to the equilibrium assumption. The uncertainty level on flow models is difficult to estimate because the variation of NO concentration with the reservoir enthalpy is strongly nonlinear regardless of the assumptions.[22]

Thermochemical Model

Let us summarize the available information about the nozzle-flow thermochemistry.

1) The nozzle wall-pressure distributions are close to the values given by the equilibrium model at high enthalpy.

2) The Electre sphere-cone pressure distributions indicate also that the freestream Mach number is close to equilibrium and then the pressure and the translational temperature are close to equilibrium values, too. (Also, the pressure and the translational temperature must vary similarly because of the mass-flow conservation and the equation of state.)

3) The DLAS technique gives translational temperature values close to equilibrium values and even larger.

4) The DLAS technique gives NO concentrations much closer to frozen-nonequilibrium than to equilibrium values.

5) It is difficult to draw conclusions about the DLAS and pseudospark techniques for obtaining freestream velocity because of the low sensitivity of this parameter to the thermochemistry with regard to the uncertainties, although DLAS results seem to be generally close to frozen and nonequilibrium models.

6) All of these observations are fully repeatable, regardless of the arc-chamber option (copper or carbon).

7) It has been not discussed here, but the comparisons of Navier–Stokes shock layers with schlieren images tend to demonstrate that the flows around models are driven by conventional nonequilibrium kinetics.[2, 12, 25, 41]

The apparent relaxation to equilibrium of the nozzle flow that could be indicated by static pressure and translational temperature behavior is in contradiction to conventional assumptions about high-enthalpy flows in large-area-ratio nozzles, i.e., the freezing of the thermochemistry beyond the throat. We have not found in the literature abundant experimental results for a high-enthalpy nozzle at conditions close to the present ones. It is clear that conclusions on the thermochemistry are not possible when only pitot pressure and enthalpy measurements are available. Reference 42 consists probably of the most exhaustive study concerning high-enthalpy nozzle expansions. Arc-jet nozzle flows are studied, some of them with numerous spectroscopic data, but for low reservoir pressures compared to F4 and/or low area ratios, so that it is difficult to transpose the results to F4.

We see two possible reasons for the F4 nozzle-2 apparent relaxation of translational temperature and pressure to equilibrium. First, it can be due to the quenching effect of some flow contaminant, efficient at a very small amount (because of the full repeatability). A way to check this point could be to reproduce F4 experiments in other high-enthalpy facilities, working with a different principle from that in the F4, e.g., shock tunnels, unless this contaminant also is present in the other facility. The second reason can be that what is observed in the F4 nozzle proceeds directly from the physics of flow expansion. In this case, what could be the relevant thermochemical model? The following principle is proposed: Vibration–dissociation couplings have been proposed largely for flow behind shock waves; a molecule vibrating at a high level dissociates easier than a molecule vibrating at a low level. A higher vibrational level means a smaller energy to be brought by the collision partner and a larger collisional cross section, all of this resulting in a faster dissociation rate. In flows dominated by recombination reactions such as nozzle expansions, the recombination of two atoms to a molecule vibrating at a high level seems easier than the recombination to a molecule vibrating at a low level because the collision partner will have to evacuate a smaller energy, making the recombination more likely to occur and resulting in a faster recombination rate. This acceleration of recombination rates by vibrational effect usually is not accounted for in nozzle computations because the recombination rates are computed only with the translational temperature. This effect has been introduced in the one-dimensional Euler code in thermochemical nonequilibrium[26] as follows. For a dissociation reaction, the forward rate k_f depends on an averaged temperature T_a as

$$k_f = k_f(T_a) \tag{3}$$

$$T_a = T^q T_v^{(1-q)} \tag{4}$$

where q is a coefficient between 0 and 1. Equations (3) and (4) represent the vibration–dissociation coupling as formulated by Park.[39] To take into account the vibrational influence on the recombination (backward) rate k_b, the following relationship is proposed, according to the principle of microscopic reversibility[43]:

$$k_b = k_f(T_a)/K_e(T) \tag{5}$$

where $K_e(T)$ is the equilibrium constant computed at the translational temperature. For convenience, this vibration–dissociation–recombination coupling is denoted VDR.

In the following preliminary analysis, q is a constant equal to 0.5 (q also can be expressed as a function of translational/vibrational temperature ratio[44]). VDR was activated on N_2 and O_2 recombination reactions. No VDR was set on NO in this first approach because the NO amount is generally small at the nozzle exit and NO formation proceeds also from exchange reactions. NO is assumed at vibrational equilibrium. An Euler computation was performed with the one-dimensional code. The computational case is the same as in Fig. 11, i.e., run 842 at 40 ms, $P_i = 404$ bar, $H_i/RT_0 = 170$. The one-dimensional Euler calculation results are compared with results calculated from corresponding equilibrium and nonequilibrium conditions without VDR and with experimental results when possible (Figs. 18–24).

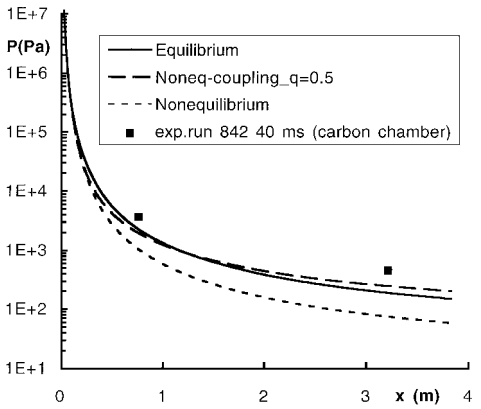

Fig. 18 Nozzle-pressure distributions from experimental runs and one-dimensional Euler computations at equilibrium and at nonequilibrium with and without VDR ($P_i = 404$ bar, $H_i/RT_0 = 170$).

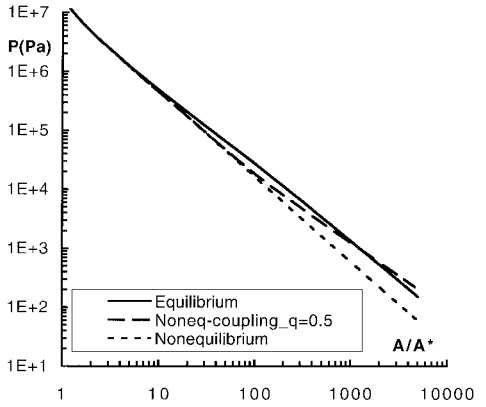

Fig. 19 Nozzle-pressure distributions vs area ratio from one-dimensional Euler computations at equilibrium and at nonequilibrium with and without VDR (P_i = 404 bar, H_i/RT_0 = 170).

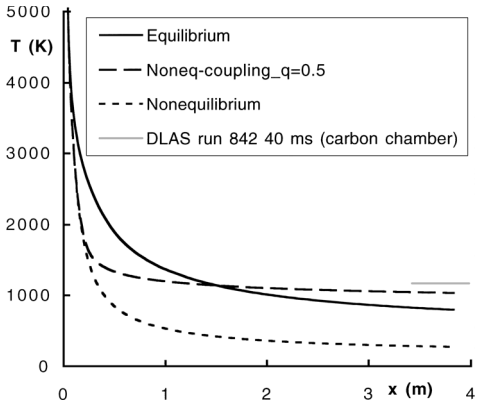

Fig. 20 Nozzle translational-temperature distributions from experimental runs and one-dimensional Euler computations at equilibrium and at nonequilibrium with and without VDR (P_i = 404 bar, H_i/RT_0 = 170).

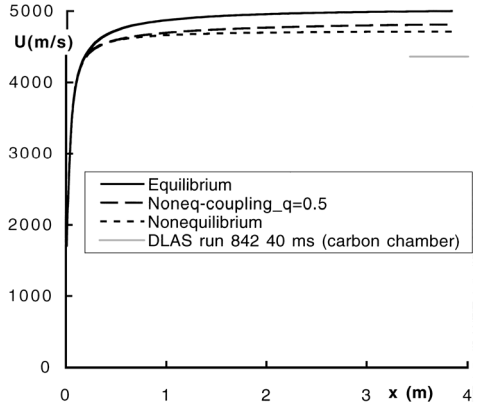

Fig. 21 Nozzle velocity distributions from experimental runs and one-dimensional Euler computations at equilibrium and at nonequilibrium with and without VDR (P_i = 404 bar, H_i/RT_0 = 170).

Pressure

Pressure distributions are given in Fig. 18 as a function of axis coordinate and in Fig. 19 as a function of the area ratio. In Fig. 18, the nonequilibrium-with-VDR result is found close to the equilibrium curve and close to the experimental data (with respect to the boundary-layer absence). Figure 19 shows that the equilibrium distribution diverges from the others for area ratio smaller than 10, whereas the deviation between the nonequilibrium distribution and nonequilibrium-with-VDR distribution occurs for an area ratio of the order of 100 because some length is needed for the difference between vibrational and translational temperatures to become significant.

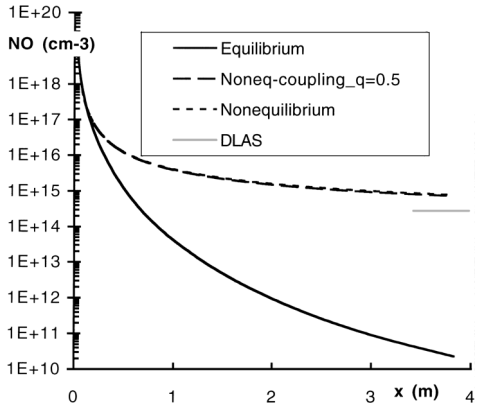

Fig. 22 Nozzle NO concentration distributions from experimental runs and one-dimensional Euler computations at equilibrium and at nonequilibrium with and without VDR (P_i = 404 bar, H_i/RT_0 = 170).

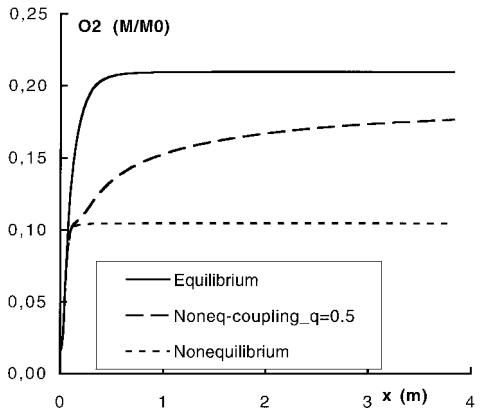

Fig. 23 Nozzle O_2 concentration distributions from one-dimensional Euler computations at equilibrium and at nonequilibrium with and without VDR (P_i = 404 bar, H_i/RT_0 = 170).

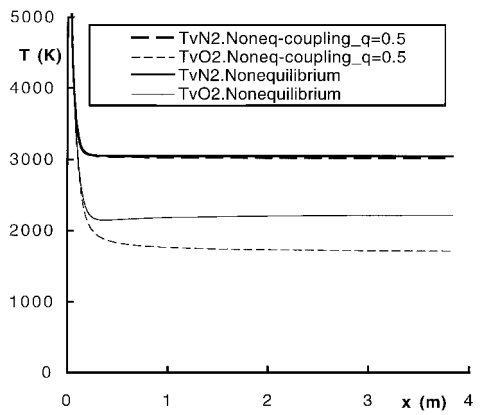

Fig. 24 Nozzle O_2 and N_2 vibrational temperature distributions from one-dimensional Euler computations at equilibrium and at nonequilibrium with and without VDR (P_i = 404 bar, H_i/RT_0 = 170).

Freestream Translational Temperature

Translational-temperature distributions for the three computations and the DLAS results are compared in Fig. 20. As for pressure, the nonequilibrium-with-VDR case is the closest to equilibrium and experimental values.

Freestream Velocity

The velocity comparison is displayed in Fig. 21. The nonequilibrium distribution is the closest to experimental values and to the nonequilibrium-with-VDR distribution.

Freestream NO Concentration

NO concentrations, in molecules/cm^3, are given in Fig. 22. Because NO was assumed to be at vibrational equilibrium and, therefore, no VDR was present on NO chemical reactions, nonequilibrium NO concentrations with and without VDR are very similar. In the test section ($x > 342$ cm), nonequilibrium and DLAS NO concentrations correspond to 5 and 2% in mole fraction, respectively.

Freestream Oxygen Concentration

Computed molecular oxygen concentrations are shown in Fig. 23. The VDR distribution is located between nonequilibrium and equilibrium results.

Freestream Vibrational Temperatures

Finally, computed vibrational temperatures at nonequilibrium with and without VDR are given in Fig. 24. It appears that T_v N_2 is weakly affected by VDR because the chemistry on N_2 is not very active in the expansion. T_v O_2 shows more sensitivity to VDR, although at the nozzle exit, T_v O_2 stays significantly higher than the corresponding translational temperature in Fig. 20.

These modeling and comparison works yield three remarks.

1) The statement "close-to-equilibrium" that has been attached to some F4 nozzle flow data appears actually to be a question of definition. In effect, the static enthalpies at nozzle exit computed according to the three models—from equilibrium and nonequilibrium with and without VDR—represent 7, 14, and 17%, respectively, of the reservoir enthalpy. Then the model with VDR is much closer to the nonequilibrium model without VDR than to the equilibrium model in terms of energy storage in nonequilibrated modes.

2) Further measurements of vibrational temperatures could constitute a final validation of the VDR model. If the apparent relaxation to equilibrium of the nozzle flow is caused by some flow contamination, it is likely that this relaxation also will affect the vibrational temperatures. Conversely, if further measurements give high values of vibrational temperatures compared with the translational temperature, it will be an important step in the model validation process. In fact, the basic problem for model validation is to know when there are enough experimental data to be sure that the theoretical interpretation can be unique. It will involve additional sensitivity studies. Measurements of N_2 vibrational temperatures with the coherent anti-Stokes Raman scattering technique[45] and EBF spectroscopy are planned within one year. It is not clear which techniques could be applied to measure oxygen concentration and vibrational temperature.

3) The VDR model discussed here must be considered as preliminary. Theoretical refinements will be performed once more experimental data are available, in particular concerning vibrational temperatures, and once the VDR relevance is demonstrated.

Conclusion

The analysis of experimental results obtained in the F4 wind tunnel has contributed to the addressing of problems of first importance of for this type of wind tunnel and for high-enthalpy testing in general, i.e., the determination of the reservoir enthalpy and the thermochemical nature of the nozzle flow in the test section.

The problem of the reservoir enthalpy determination can be considered now as solved. Several techniques are available, based on heat-transfer-rate measurements (spherical probes of different diameters and conical probe) or advanced optical measurements (Doppler effect with DLAS and time-of-flight with EBF). Measurements of reservoir enthalpy (or freestream velocity) with these techniques are in very good agreement in the case of low flow contamination, i.e., when using the new carbon arc chamber in place of the conventional copper arc chamber.

Concerning the thermochemical nature of the nozzle flow, the analysis of several types of experimental results (nozzle wall pressure, sphere–cone model pressure distributions, DLAS translational temperature, and NO concentration) yields the undoubted conclusion that freestream data as translational temperature and pressure are close to equilibrium at high-enthalpy conditions. However, the DLAS NO concentrations are the closest to nonequilibrium values. Thanks to the full repeatability of the experimental measurements, regardless of the arc chamber option, it is very likely that such nozzle flow behavior is caused by the physics of flow expansion and not by the quenching of some contaminant. The cross checking of F4 experiments with experiments in other high-enthalpy facilities, working with a principle different from that of F4, such as shock tunnels, at conditions and nozzle area ratio close to those of the F4, would help to verify this assumption and would be very welcome. A thermochemical nonequilibrium model, involving a coupling between vibration, dissociation, and recombination, is demonstrated as capable of reproducing available experimental data. Further measurements of vibrational temperatures, linked to additional sensitivity studies, would demonstrate the model relevance and then allow model refinement studies.

Acknowledgments

Most of the presented work has been sponsored by the European Space Agency. The authors also want to thank ONERA staff from the Physics Department and the Large Testing Facilities Department who performed the experiments in F4.

References

[1]Sagnier, P., "Synthesis of the Hyperboloïd-Flare Campaign in F4 (January–February 1994)," ONERA, RT 70/6121 SY, Châtillon, France, Dec. 1994.

[2]Sagnier, P., Joly, V., and Marmignon, C., "Analysis of Nonequilibrium Flow Calculations and Experimental Results Around a Hyperboloïd-Flare Configuration," *Proceedings of the Second European Symposium on Aerothermodynamics for Space Vehicles*, ESA SP-367, European Space Technology and Research Centre, Noordwijk, The Netherlands, 1995, pp. 491–496.

[3]Vérant, J.-L., "Numerical Enthalpies Rebuilding for Perfect Gas and Nonequilibrium Flows. Application to High Enthalpy Wind Tunnels," ONERA, RT 69/6121 SY, Châtillon, France, Sept. 1994.

[4]Fay, J. A., and Riddell, F. R., "Theory of Stagnation Point Heat Transfer in Dissociated Air," *Journal of the Aeronautical Sciences*, Vol. 25, No. 2, 1958, pp. 73–85.

[5]Bertin, J. J., "General Characterization of Hypersonic Flows," 1st Joint Europe–US Short Course on Hypersonics: GAMNI-SMAI (Groupe pour l'Avancement des Méthodes Numériques de l'Ingénieur—Société de Mathématiques Appliquées Industrielles) and Univ. of Texas at Austin, Paris, France, Dec. 1987.

[6]Miller, C. G., "Laminar Heat-Transfer Distributions on Biconics at Incidence in Hypersonic-Hypervelocity Flows," NASA TP 2213, 1985.

[7]Lees, L., "Laminar Heat Transfer over Blunt-Nosed Bodies at Hypersonic Flight Speeds," *Jet Propulsion*, Vol. 26, No. 4, 1956, pp. 259–269.

[8]Sagnier, P., "Comparison of Nozzle Flow Simulations with LDIAS Measurements Obtained During the Manned Space Transportation Program Phase 1 F4 Nozzle#2 Calibration Campaign," ONERA, RT 74/6121 SY, Châtillon, France, July 1995.

[9]Pope, R. B., "Stagnation-Point Convective Heat Transfer in Frozen Boundary Layers," *AIAA Journal*, Vol. 6, No. 4, 1968, pp. 619–626.

[10]Sagnier, P., "Synthesis of Manned Space Transportation Program Phase 1 F4 nozzle#2 Calibration Campaign," ONERA, RT 84/6121 SY, Châtillon, France, Feb. 1996.

[11]Pélissier, C., "F4 Calibration Tests—Phase 2 (Study n° 4709 GY 740 G)," ONERA, Test Rept. 4709 GY 740 G-01, Châtillon, France, July 1996.

[12]Sagnier, P., "Synthesis of the Electre Standard Model Numerical and Experimental Activities at ONERA," ONERA, RT 7/8908 GY, Châtillon, France, Jan. 1996.

[13]Vérant, J.-L., and Sagnier, P., "Assessment of Total Conditions and Flow Thermochemical Nature in the ONERA High Enthalpy Wind Tunnel," AIAA Paper 96-2239, June 1996.

[14]Sagnier, P., Masson, A., Mohamed, A. K., Vérant, J.-L., and Devezeaux, D., "Synthesis of Manned Space Transportation Program Calibration Campaigns in ONERA F4 Hot Shot Wind Tunnel," *International Congress on Instrumentation in Aerospace Simulation Facilities* (Wright–Patterson AFB, OH), *ICIASF'95 Record 95-CH3482-7*, Inst. of Electrical and Electronics Engineers, Piscataway, NJ, 1995, pp. 49.1–49.8.

[15]Soutadé, J., "Direct Measurement of the Velocity in the F4 Wind Tunnel with the Pseudospark Electron Gun, and with the Electre Model in the Test Section (Study n° 8057 GH 740 G)," ONERA, Test Rept. PV 1/8057 GY, Châtillon, France, April 1997.

[16]Soutadé, J., "Tests of the Hyperboloïd-Flare Model with a Direct Velocity Measurement Device in the F4 Wind Tunnel (Study n° 8046 GH 740 G)," ONERA, Test Rept. PV 1/8046 GY, Châtillon, France, May 1997.

[17]Mohammed, A., Rosier, B., Sagnier, P., Henry, D., and Louvet, Y., "Applications of Infrared Diode Laser Absorption Spectroscopy to the F4 High Enthalpy Wind Tunnel," *Aerospace Science and Technology* (to be published).

[18]Sagnier, P., "Synthesis of 1997 Electre and Hyperboloïd-Flare F4 Test Campaigns," ONERA, RT 95/6121 SY, Châtillon, France, Aug. 1997.

[19]Sagnier, P., Vérant, J.-L., Devezeaux, D., Mohamed, A. K., and Masson, A., "Real Gas Flow Characterization in the ONERA F4 High Enthalpy Wind Tunnel," *17th International Congress on Instrumentation in Aerospace Simulation Facilities* (Monterey, CA), *ICIASF'97 Record 97CH36121*, Inst. of Electrical and Electronics Engineers, Piscataway, NJ, 1997, pp. 378–388.

[20]Marinelli, W. J., Kessler, W. J., Allen, M. G., and Davis, S. J., "Copper Atom Bases Measurements of Velocity and Turbulence in Arc Jet Flows," AIAA Paper 91-0358, Jan. 1991.

[21]Bamford, D. J., O'Keefe, A., Babikian, D. S., Stewart, D. A., and Strawa, A. W., "Characterization of Arc-Jet Flows Using Laser Induced Fluorescence," AIAA Paper 94-0690, Jan. 1994.

[22]Sagnier, P., "F4 Nozzle#2 Exit Flow Charts for Air and Nitrogen," ONERA, RT 71/6121 SY, Châtillon, France, Dec. 1994.

[23]Sagnier, P., and François, G., "Analysis of Calibration Results in High-Enthalpy F4 Hot-Shot Wind Tunnel," *Proceedings Shock Waves@Marseille I, Hypersonic, Shock Tube & Shock Tunnel Flow*, Springer–Verlag, Berlin, 1995, pp. 233–238.

[24]Sagnier, P., "Summary of Computations on the Electre Standard Model in the Frame of Test Campaigns in ONERA Wind Tunnels, F4, R3Ch, S4MA," ONERA, RT 6/8908 GY, Châtillon, France, Oct. 1995.

[25]Sagnier, P., and Kordulla, W., "Synthesis of Contributions to the Electre Test Cases Within the Fourth European High-Velocity Database Workshop (Noordwijk, The Netherlands)," ONERA, RT 73/6121 SY, Pt. 1/2, Châtillon, France, Sept. 1995.

[26]Sagnier, P., and Marraffa, L., "Parametric Study of Thermal and Chemical Nonequilibrium Nozzle Flow," *AIAA Journal*, Vol. 29, No. 3, 1991, pp. 334–343.

[27]Edenfield, E. E., "Design of a High Reynolds Number Mach Number 8 Contoured Nozzle for the Hypervelocity Wind Tunnel (F)," AEDC-TR-72-48, Aug. 1972.

[28]Hachemin, J.-V., and Vérant, J.-L., "3-D Parallel Multi-Blocks Thermo-Chemical Nonequilibrium Simulation with a PNS Solver," *Proceedings of the Second European Symposium on Aerothermodynamics for Space Vehicles*, ESA SP-367, European Space Technology and Research Centre, Noordwijk, The Netherlands, 1995, pp. 141–148.

[29]Hachemin, J.-V., "Development of Parabolized Navier–Stokes Code for 3D Thermochemical Nonequilibrium Flows," Ph.D. Thesis, Mechanics Dept., Univ. of Poitiers, Poitiers, France, 1996.

[30]Van Leer, B., "Flux Splitting for Euler Equations," *Lecture Notes in Physics*, Vol. 170, 1982, pp. 507–512.

[31]Yee, H. C., and Harten, A., "Implicit TVD Schemes for Hypersonic Conservation Laws in Curvilinear Coordinates," AIAA Paper 85-1513, July 1985.

[32]Osher, S., and Solomon, F., "Upwind Difference Schemes for Hyperbolic Systems of Conservation Laws," *Mathematics of Computations*, Vol. 38, No. 158, 1982, pp. 339–374.

[33]Coquel, F., and Liou, M.-S., "Hybrid Upwind Splitting (HUS) by a Field-by-Field Decomposition," NASA TM 106843, Jan. 1995.

[34]Carrière, P., "Méthodes Théoriques d'Étude des Écoulements Supersoniques," *Publications Scientifiques et Techniques du Ministère de l'Air*, 339a, Service de Documentation Scientifique et Technique de L'Armement, Paris, France, 1964.

[35]Vérant, J.-L., and Sagnier, P., "F4 and HEG Nozzle Viscous Computations: Outlet Conditions Assessment," ONERA, RT 78/6121 SY, Châtillon, France, Dec. 1995.

[36]Hollanders, H., and Marmignon, C., "Navier–Stokes High-Speed Flow Calculations by an Implicit Non-Centered Method," AIAA Paper 89-0282, Jan. 1989.

[37]Coquel, F., and Marmignon, C., "Roe Type Linerarization for the Euler Equations for Weakly Ionized Multicomponents and Multi-Temperatures Gas," AIAA Paper 95-1675, June 1995.

[38]Hannemann, K., "Computation of the Flow in Hypersonic Wind Tunnel Nozzles (Contribution to the Fourth European High Velocity Database Workshop)," DLR, Rept. IB 223-95 A 47, Göttingen, Germany, June 1996.

[39]Park, C., "Assessment of Two-Temperature Kinetic Model for Ionizing Air," AIAA Paper 87-1574, June 1987.

[40]Millikan, R. C., and White, D. R., "Systematics of Vibrational Relaxation," *Journal of Chemical Physics*, Vol. 39, No. 12, 1963, pp. 3209–3213.

[41]Sagnier, P., and Vérant, J.-L., "Validation of High Enthalpy Wind Tunnel Simulations," *Computational Methods in Applied Sciences'96*, Wiley, Chichester, England, UK, 1996, pp. 317–323.

[42]Park, C., and Lee, S. H., "Validation of Multi-Temperature Nozzle Flow Code NOZNT," AIAA Paper 93-2862, July 1993.

[43]Candler, G., "Translation-Vibration-Dissociation Couplings in Nonequilibrium Hypersonic Flows," AIAA Paper 89-1739, June 1989.

[44]Hansen, C. F., "Vibrational Noequilibrium Effects on Diatomic Dissociation Rates," *AIAA Journal*, Vol. 31, No. 11, 1993, pp. 2047–2051.

[45]Grisch, F., Bouchardy, P., Koch, U., and Gülhan, A., "Rotational and Vibrational Temperature and Density Measurements by Coherent Anti-Stokes Raman Scattering in a Nonequilibrium Flow," RTO/AGARD Fluid Dynamics Panel Symposium, Advanced Aerodynamic Measurement Technology, ONERA Print TP 1997-166, Seattle, WA, Sept. 1997.

W. Oberkampf
Associate Editor